Azerag et al. International Journal of Mechanical and Materials Engineering

DOI 10.1186/s40712-015-0045-8

International Journal of Mechanical and Materials Engineering
a SpringerOpen Journal

ORIGINAL ARTICLE Open Access

Structural properties of batch foamed acrylonitrile butadiene styrene/nanoclay nanocomposites

Bashar Azerag[1], Taher Azdast[1*], Ali Doniavi[1], Sajjad Mamaghani Shishavan[1] and Richard Eungkee Lee[2]

Abstract

Background: Present study investigates the effect of adding nanoclay particles and foaming conditions on cellular properties of ABS/Nanoclay nanocomposite foams.

Methods: For this purpose, first nanocomposite components are mixed using a twin-screw extruder. The amount of added nanoclay is considered 2 and 4 percentage by weight. Also, poly methyl methacrylate (PMMA) with the percentages of 2 and 4 wt% are used as the compatibilizer. Distribution of nanoclay particles in ABS matrix is examined using X-ray diffraction test. Then, nanocomposite samples are produced using injection molding process and foamed using batch foaming process. CO_2 gas is used as the physical blowing agent of the foaming process. The saturation time of samples and the effect of adding of nanoclay on CO_2 sorption/desorption rate was assessed by gravimetric method prior to foaming experiments. Then, nanocomposite samples are foamed under different process conditions according to a Taguchi L9 orthogonal array.

Results: The obtained results reveal that adding nanoclay increases the cell density and decreases both foam density and cell size of ABS/nanoclay composite foams compared to the pure ABS foams.

Conclusions: Results show that the structural properties of nanocomposite foams depend on both processing parameters and percentage of nanoclay in the nanocomposite specimens.

Keywords: ABS; Clay; Nanocomposite; Foam; Batch; Microcellular; Taguchi

Background

Foaming is the creation of tiny bubbles into a polymer structure using gas penetration and solution as the physical blowing agent into the polymer matrix, and it is also the creation of a thermodynamic instability by reducing pressure and increasing temperature. Microcellular foams are defined as foams with a cell diameter lower than 10 μm and cell density more than 10^{10} cells/cm^3 (Jacobs et al. 2008). The cell radius of microcellular foams is less than the natural critical crack of a polymer; therefore, polymer weight can be reduced without having a negative effect on mechanical properties compared to traditional foams. Martini and Suh at Massachusetts Institute of Technology (MIT) in 1981 introduced microcellular foams as a means to reduce the amount of plastic materials without sacrificing their functionality (Martini 1981). Batch microcellular foaming contains a saturated sample under non-reaction gas pressure in reservoir pressure until equilibrium gas concentration is achieved. Then the pressure is discharged, and samples are immersed in hot oil with temperatures approaching the transition temperature of the polymer. There is no doubt that foam expansion continues until polymer viscosity increases or all available supercritical fluid is used. Carbon dioxide (CO_2) and nitrogen (N_2) are the most common supercritical fluids in the microcellular foaming process used as physical blowing agents. They are eco-friendly, non-toxic, cheap, and abundant. However, the permeability and solubility of CO_2 in the polymers are higher than those of N_2, and the supercritical parameters of CO_2 are easily available (Tc = 31.1 °C, Pc = 73.8 bar) (James et al. 2005; Lee et al. 2007). Acrylonitrile butadiene styrene (ABS) is an amorphous co-polymer wherein acrylonitrile brings chemical resistance and heat stability, butadiene brings toughness, and styrene provides good processing characteristics. The

* Correspondence: t.azdast@urmia.ac.ir
[1]Mechanical Engineering Department, Faculty of Engineering, Urmia University, Urmia, Iran
Full list of author information is available at the end of the article

Table 1 Characteristics of the ABS used in the present study

Property	Unit	Test method	Typical value
Melt flow index (200 °C/5 kg)	gr/10 min	ASTM D-1238	1.7
Izod impact strength (notched)	Kgf.cm/cm	ASTM D-256	22
Vicat softening yield	°C	ASTM D-1525	99
Tensile strength at yield	Kgf/cm^2	ASTM D-638 (5 mm/min)	440
Elongation at break	%	ASTM-638 (5 mm/min)	40
Rockwell hardness (at 23 °C)	R. scale	ASTM D-785	104
Density	gr/cm^3	Archimedes	1.04

foamed polymers' structure including nanoparticles as nanofillers has been improved with reduced flammability properties, reduced gas permeability, increased strength-to-weight ratio, increased impact resistance, long fatigue life, and better thermal and electrical insulation properties compared to unfoamed polymers. Nanofillers can be used as a nucleation agent in the gas foaming process, but they are also known to promote the heterogeneous nucleation of extra cells during foaming; hence, polymer/clay nanocomposite foams are usually characterized by a small cell size and high cell density (James et al. 2005). Okamoto et al. used organically modified layered silicates as nucleating agents to produce polypropylene (pp)/clay composites (Okamoto et al. 2001). Yeh et al. studied the effect of dispersion capability of organoclay on cellular structure and physical properties of poly methyl methacrylate (PMMA)/clay nanocomposite foams and demonstrated that the well-dispersed clay particles in the polymer matrix cause an increase in cell density, a decrease in cell size, and also an increase in mechanical strength of PMMA/clay nanocomposite foams (Yeh et al. 2009). Mamaghani Shishavan et al. studied the mechanical properties and composition capability of ABS/PMMA/clay nanocomposites and showed that ABS and clay nanoparticles with PMMA could be compounded and their mechanical properties are stronger than those of the pure ABS (Mamaghani Shishavan et al. 2014). Urbanczyk et al. studied the batch foaming of Styrene Acrylonitrile/clay nanocomposites with CO_2 gas and illustrated that adding nanoparticles significantly increases the cell density, from 8.5×10^{11} cells/cm^3 for pure SAN foam, to 3.6×10^{12} cells/cm^3 for the intercalated nanocomposite and 7.6×10^{13} cells/cm^3 for SAN containing the exfoliated clay. Therefore, the nanoclay clearly acts as an effective heterogeneous nucleating agent (Urbanczyk et al. 2010). Papers were also found on ABS foams which were produced by supercritical fluid CO_2. An article by Murray et al. has examined batch foaming conditions of ABS with CO_2 (Murray et al. 2000). Kamran et al. studied the mechanical and microstructural properties of microcellular foams of ABS composites with CO_2 (Beydokhti et al. 2006).

The current study was carried out in order to determine the effect of adding nanoclay and foaming conditions on the structural properties of ABS/PMMA/clay

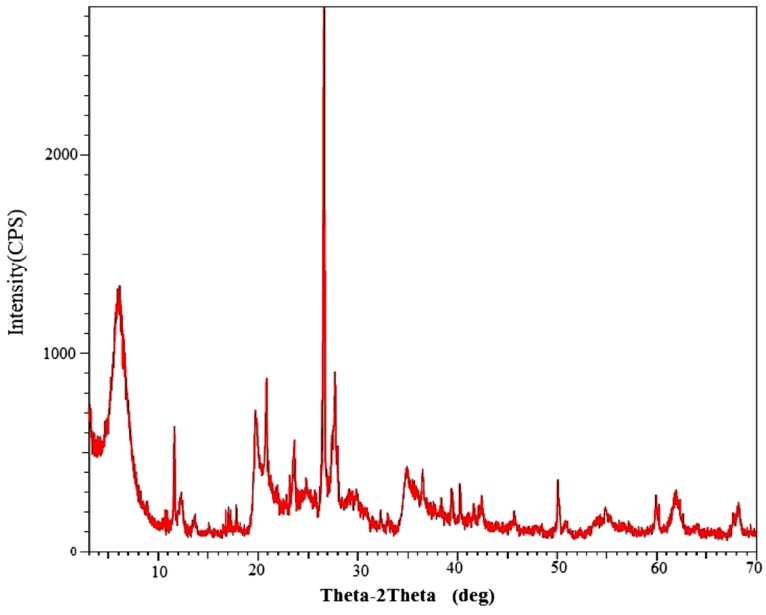

Fig. 1 X-ray diffraction diagram for Cloisite 30B

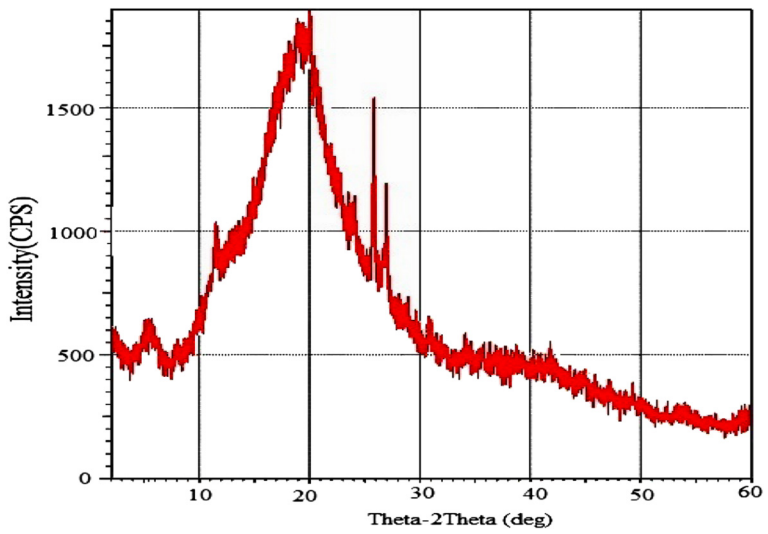

Fig. 2 X-ray diffraction diagram for nanocomposite masterbatch

nanocomposite foams such as foam density, foam expansion ratio, cell density, and cell size. For this purpose, the amount of nanoclay and processing parameters including foaming temperature, saturation pressure, and foaming time were considered in three levels (low, medium, high), and then a design of experiments was performed using the Taguchi design of experiments approach. After physically mixing the ABS and nanoclay and also PMMA as the compatibilizer, a co-rotating twin-screw extruder was used to produce ABS/nanoclay pellets. In order to examine compounding of ABS and nanoclay particles, an X-ray diffraction (XRD) test was conducted. Nanocomposite samples were then prepared using injection molding process. Afterwards, they were foamed by batch foaming process using CO_2 gas as the physical blowing agent. Cell density and cell size of foamed samples were calculated using the scanning electron microscopy (SEM) images of foamed samples.

Methods

Nanocomposite preparation

In this study, ABS co-polymer with commercial grade of Starex SD0150, with the specifications presented in Table 1, was used as the polymeric matrix of the experimentations. Montmorillonite clay with the trade name Cloisite 30B modified with a quaternary ammonium salt from Southern Clay Products, Inc. has been used as nanofillers. PMMA was also used as the compatibilizer (Mamaghani Shishavan et al. 2014; Saraeian et al. 2012). The melt intercalation method was applied to prepare ABS/PMMA/clay nanocomposite (APCN) materials. Therefore, to prepare nanocomposites with varying amounts of nanoclay (2 and 4 wt%) (Mamaghani Shishavan et al. 2014; Singh and Ghosh 2014), first, a masterbatch containing 800 g ABS, 100 g PMMA, and 100 g Cloisite 30B was dried by being placed and kept in an oven heated to 85 °C for 2 h. Then, a Collin twin-screw extruder with a length-to-diameter ratio of 45 was used to mix the nanocomposite components. In order to prepare the nanocomposite granules with the proportions mentioned above, the obtained masterbatch was diluted with the required amounts of ABS. The processing temperature and screw speed of the extruder were adjusted at 190 °C and 250 rpm, respectively. Finally, in order to produce APCN samples, the prepared granules were injected into a mold cavity according to the tensile strength standard of ASTM: D638-10 (Mamaghani Shishavan et al. 2014). Nanocomposite samples were injected at the processing parameters of 132 MPa injection pressure, 80 °C mold temperature, 15 s cooling time, 132 MPa holding pressure, and 6 s holding pressure time. In order to ensure the distribution of nanoclay particles in the polymer matrix, the obtained masterbatch and purchased nanoclay powder were scanned with an XRD machine at a scanning rate of 2° per minute and wavelength of 1.5602 Å. Clay and organoclay showed a characteristic peak in XRD analysis due to their regular layered structures. The first peak was indicative of platelet separation or *d*-spacing in clay structure. XRD pattern graphs for Cloisite 30B and nanocomposite masterbatch are shown in Figs. 1 and 2, respectively. The X-ray

Table 2 XRD results for ABS/PMMA/clay nanocomposites

Samples	2θ (deg)	*d*-spacing (nm)
Cloisite 30B	6	1.49
ABS/PMMA/clay	5.3	1.7

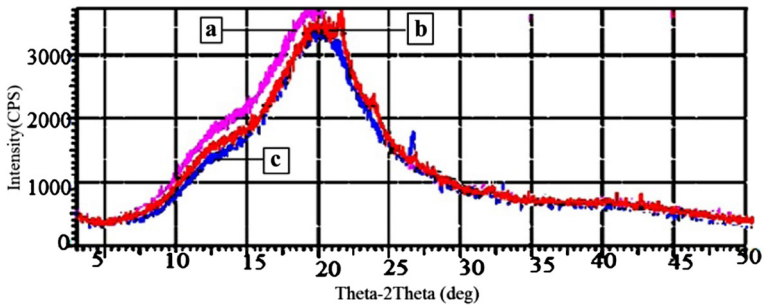

Fig. 3 XRD patterns of (*a*) pure ABS, (*b*) APCN with 2 wt%, and (*c*) APCN with 4 wt%

Table 3 Levels of process parameters and nanoclay percentage

Process parameters	Level 1	Level 2	Level 3
Nanoclay (wt%)	0	2	4
Saturation pressure (MPa)	3	4	5
Foaming temperature (°C)	80	100	120
Foaming time (s)	20	60	100

Table 4 Foaming experiments of this research

Trials	Nanoclay (wt%)	Saturation pressure (MPa)	Foaming temperature (°C)	Foaming time (s)
1	0	3	80	20
2	0	4	100	60
3	0	5	120	100
4	2	3	100	100
5	2	4	120	20
6	2	5	80	60
7	4	3	120	60
8	4	4	80	100
9	4	5	100	20

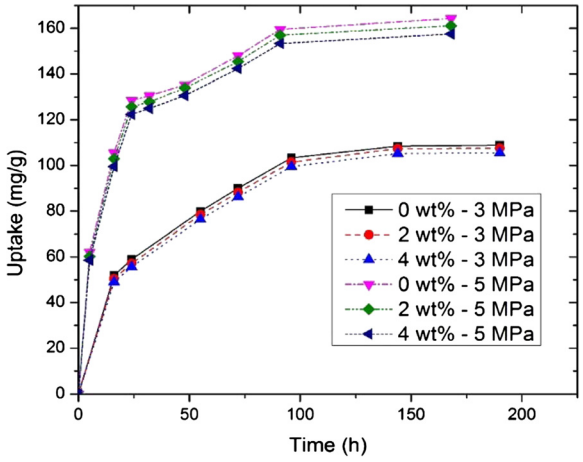

Fig. 5 CO_2 sorption curves for pure ABS and APCN materials at saturation pressures of 3 and 5 MPa

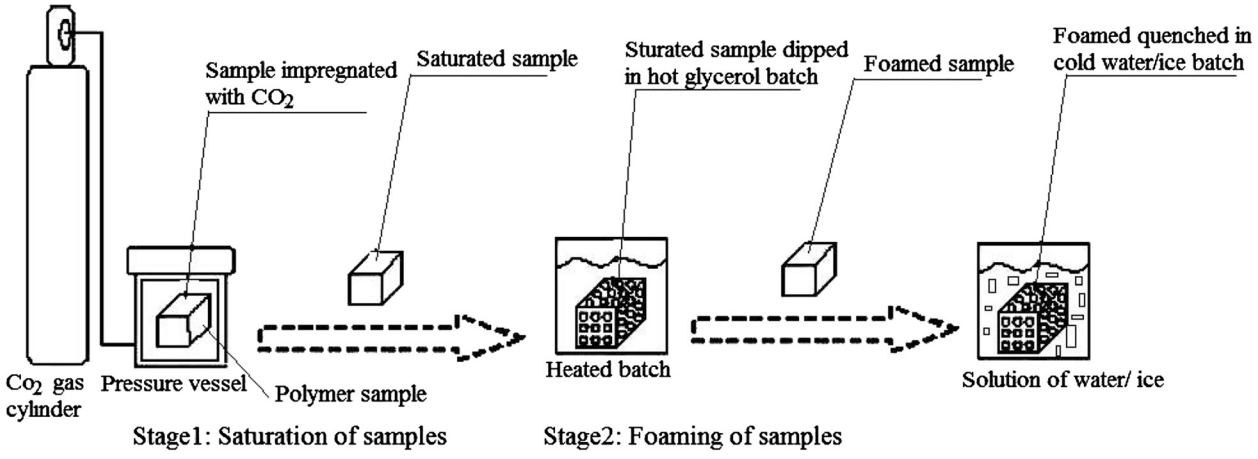

Fig. 4 Batch foaming method used to prepare APCN foam

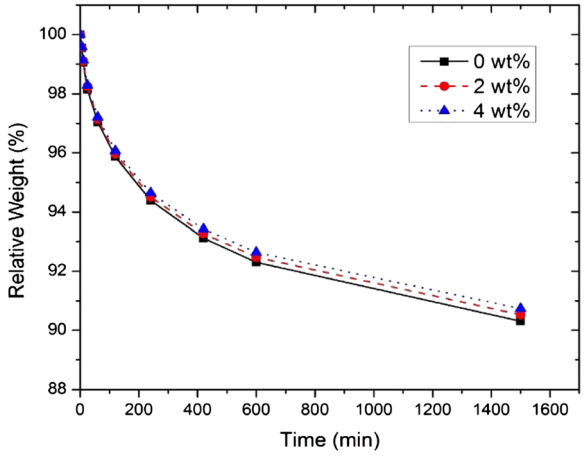

Fig. 6 Desorption curve at saturation pressure of 5 MPa and saturation time of 25 h

diffraction results are also listed in Table 2, and *d*-spacing of nanoclay layers was computed by Bragg's law as follows:

$$n\lambda = 2d\sin\theta \tag{1}$$

where n is an integer, λ is the wave length of the encountered X-ray beam, θ is the X-ray angle related to dispersion planes that is measured as the diffraction angle, and d is the distance between each of the two planes. Any change in the inner layer or *d*-spacing of the clay lattice by polymer interaction affects the position, wideness, and intensity of the characteristic peak in XRD spectra. According to Bragg's law, increasing *d*-spacing results in the broadening and shifting of the related XRD peak toward lower diffraction angles (2θ). By monitoring the position (2θ) of the characteristic peak in the nanocomposite structure, it is possible to determine the degree of intercalation/exfoliation. As presented in Table 2, while the diffraction peak of Cloisite 30B still exists in the XRD pattern graph, due to melt compounding of the clay into the ABS co-polymer, the distance between each layer of Cloisite 30B nanoclay is increased about 0.21 nm. Actually, as shown in Fig. 1, the characteristic peak of Cloisite 30B nanoclay appeared at $2\theta = 6°$ corresponding to the inner layer space; the *d*-spacing of clay layers is around 1.49 nm. To ensure the nanoclay dispersion on the ABS matrix, another XRD test was accomplished on 10 wt % masterbatch (Fig. 2). As Fig. 2 represents, there is a montmorillonite diffraction peak on $2\theta = 5.3°$ that is shifted to lower than 6°, and the nanoclay *d*-spacing increases to about 1.7 nm. This indicates that ABS chains are intercalated between the clay layers. Therefore, it is concluded that the nanoclay particles in the ABS matrix of the prepared masterbatch have an intercalated dispersion mode. After that, to survey nanoclay dispersion mode in APCN materials with 2 and 4 wt %, the XRD test was executed on pure ABS and APCN specimens that are shown in Fig. 3.

According to Fig. 3, by comparing the pattern of pure ABS and compounded samples, it is concluded that three XRD patterns are almost analogous and there is not any diffraction peak of Cloisite 30B in the range of 0°–10°. Generally, it is investigated that privation of the diffraction peak is due to the exfoliated structure and peak shift toward a lower value of 2θ is due to the intercalated structure. The lack of diffraction peak means that the distance between the silicate layer of the nanoclay is increased and a considerable amount of ABS co-polymer has been inserted into the gallery space during melt compounding. This consequence proves that the APCN samples are successfully combined in a more exfoliated and less intercalated dispersion mode (Mamaghani Shishavan et al. 2014).

Table 5 Densities of the unfoamed samples

Sample	Density (g/cm^3)
Pure ABS	1.04
ABS with 2 wt% nanoclay	1.09
ABS with 4 wt% nanoclay	1.123

Table 6 Results of foam properties for each trial of this study

Trial no.	Foam density (g/cm^3)	Relative density	Expansion ratio
T_1	0.522	0.501	1.99
T_2	0.830	0.796	1.25
T_3	0.802	0.769	1.30
T_4	0.617	0.566	1.77
T_5	0.572	0.525	1.91
T_6	0.604	0.555	1.80
T_7	0.764	0.600	1.66
T_8	0.420	0.374	2.67
T_9	0.796	0.709	1.41

CO_2 absorbency in APCNs

In order to determine the volume of absorbed CO_2, the loss rate of CO_2 gas, and saturation time, the CO_2 sorption/desorption experiments have been performed

Table 7 The response table of S/N ratios for sample density

Parameters	Level 1	Level 2	Level 3
Nanoclay percentage	3.063	4.474	4.311
Saturation pressure	4.424	4.675	2.750
Foaming temperature	5.848	2.606	3.394
Foaming time	4.160	3.146	4.545

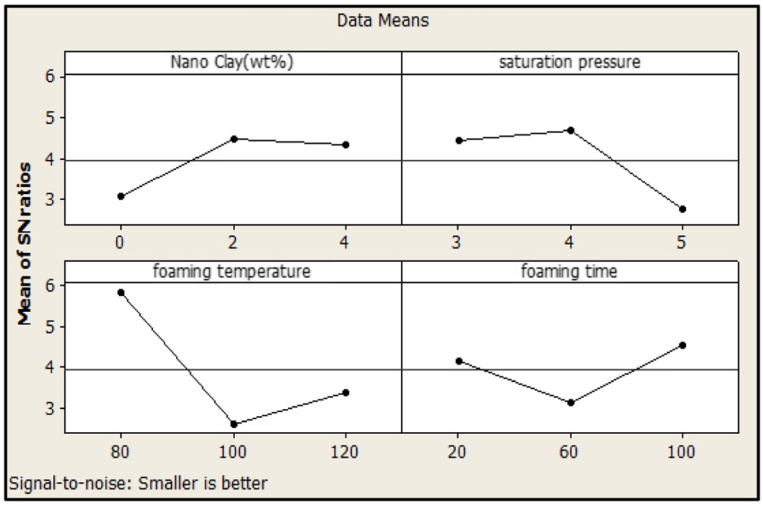

Fig. 7 S/N ratio diagram of different parameters for sample density

using an ex situ gravimetric method called mass-loss analysis. To determine the rate of gas sorption, first, APCN samples were saturated by CO_2 at certain pressure and room temperature for a determined sorption time. Then, the pressure was released and the saturated samples were promptly weighted by accurate balance (Mettler Toledo AG204, precision 0.0001 g) at room temperature. To determine the rate of gas desorption, saturated samples were weighted quickly after the discharge pressure in different times. The nanoclay effect on CO_2 absorption/desorption rates was also examined. The weight percentage of CO_2 absorbed at saturation time ($W_{gas,\,t}$) can be calculated from the sample weight at the same time (W_t) and the initial sample weight (W_i) according to the Eq. 2.

$$W_{gas,t} = \frac{W_t - W_i}{W_i} \times 100 \quad (2)$$

Design of experiments

In order to study the influence of effective factors including processing parameters and nanoclay percentage on structural properties of foamed samples, the Taguchi approach has been chosen in the design of the experiments of this study. Statistical software, Minitab16.2, is used in order to obtain the optimal levels of process parameters and nanoclay amount. The best set of factor combination could be determined using the signal-to-noise (S/N) ratio. Furthermore, the analysis of variance (ANOVA) method has been applied in order to calculate the percentage contribution of the variable factors. Process parameters such as saturation pressure, foaming time, foaming temperature, and weight percentage of the nanoclay were considered in three levels according to Table 3. Then APCN samples were foamed according to Table 4 based on a Taguchi L_9 orthogonal array.

Table 8 ANOVA table for foam density

Parameter	*f*	*s*	*v*	*P*%
Nanoclay percentage	2	23.4×10^{-3}	11.7×10^{-3}	15
Saturation pressure	2	33×10^{-3}	16.5×10^{-3}	21
Foaming temperature	2	85.9×10^{-3}	42.95×10^{-3}	55
Foaming time	2	14.3×10^{-3}	7.15×10^{-3}	9
Pooled error	0	0	0	–
Total	8	156.6×10^{-3}	–	100

Foaming process

The microcellular foaming process consists of three steps: gas absorption, nucleation, and cell growth. In the first stage, the polymeric sample is placed in a chamber pressurized by a gas as physical blowing agent at ambient temperature. The gas molecules diffuse into the polymer matrix and continue until the polymer is completely saturated with the gas. After saturation, gas absorption is interrupted and the gas distribution becomes uniform. Typically, gas sorption takes several hours or days to saturate a thin plastic sheet. Saturation time depends on the plastic materials, gas diffusivity in the plastic, sample thickness, saturation temperature, and saturation pressure.

Table 9 Results of confirmation test for optimal condition

Nanoclay (wt%)	Density (g/cm^3)	Relative density	Expansion ratio
2	0.348	0.319	3.13

Afterward, to ensure about the samples' saturation completion, the gas pressure dropped to ambient pressure, and then the saturated sample was placed in a liquid bath at a certain temperature. The thermodynamic instability, which occurred due to this sudden decrease in pressure and increase in temperature, causes thousands of cell nucleation (Colton and Suh 1987). Cell development can be controlled by adjusting the foaming temperature and foaming time.

APCN foams were prepared using solid-state foaming technology as shown in Fig. 4. Firstly, samples were saturated with CO_2 gas as physical blowing agent at ambient temperature for 120 h under a certain pressure, i.e., saturation pressure. In the next step, the pressure discharge and samples were immediately removed from the vessel pressure. Foam expansion was inducted by immersion of the saturated sample in the hot oil (glycerol) at a certain temperature (foaming temperature) and time (foaming time). Finally, foam structure was stabilized by cooling in ice/water solution. The saturation pressure, foaming temperature, and foaming time values were considered as presented in Table 4.

Foam characterization

The density of the foamed and unfoamed samples was measured by the Archimedes method as follows: Assume that a vessel containing water with a density of ρ_w is placed on a precision scale. If a sample with a mass of M_f and volume of V_f is immersed in water in such a way that the whole surface of the sample is covered by water, the scale will indicate the change in the mass (i.e., ΔM). When the sample is submerged, ΔM is equal to the weight of water that is displaced. The density is calculated from the Eq. 3 by reading the change in the mass from the scale when the sample has been submerged. The water density, ρ_w, is clear and the samples' mass, M_f, is measured before submergence. Then, for APCN foam samples of each experiment, density, relative density (ρ_f/ρ_s) where ρ_f and ρ_s are the foamed and solid sample densities, respectively, and the percentage of volume expansion are calculated.

$$\rho_f = \frac{M_f}{V_f} = \frac{M_f}{\Delta M} \times \rho_w \tag{3}$$

APCN foam porosity was observed by SEM (TESCAN MIRA3-FEG). To prepare specimens for SEM observation, the samples were dipped into liquid nitrogen and immediately fractured. Then, they were coated by gold. Image analysis was manually executed on the basis of SEM pictures by measuring the cells' size. Cell density (N_{cell}) relative to the unfoamed polymer is estimated according to Eq. 4 as shown below:

$$N_{cell} = \left(\frac{nM^2}{A}\right)^{3/2} \times \frac{\rho_s}{\rho_f} \tag{4}$$

where n is the number of cells in the SEM picture, M is the magnification size, A is the surface area of the picture (cm^2), and ρ_s and ρ_f are the solid and foamed sample densities, respectively (Zhai et al. 2006).

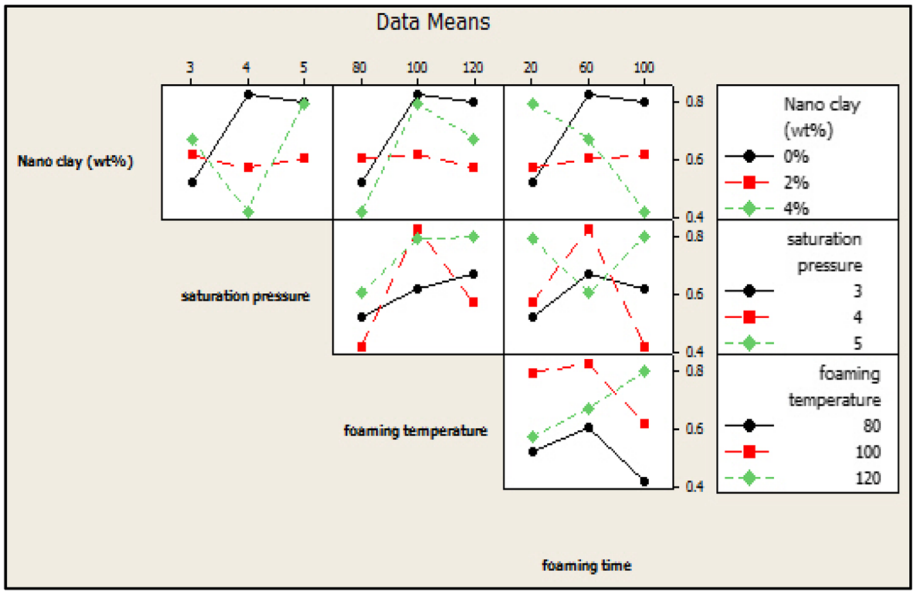

Fig. 8 Interaction plot of processing parameters for sample density

Results and discussion

CO_2 solubility and diffusivity in APCN

In order to determine the saturation time for the foaming process, CO_2 diffusivity in APCN samples has been studied. CO_2 solubility values were extracted from CO_2 sorption/desorption curves that were dependent on the saturation pressure. The nanoclay effect on sorption/desorption rates also was assessed. CO_2 sorption curves for pure ABS and different APCN samples at saturation pressures of 3 and 5 MPa are shown in Fig. 5. According to Fig. 5, maximum CO_2 sorption values related to polymer weight in pure ABS at saturation pressures of 3 and 5 MPa are 108 and 165 mg/g, respectively, while in the same situation, for APCN samples, these values (i.e., maximum CO_2 sorption) were a little bit lower than the pure ABS samples. In fact, in a constant saturation pressure, the CO_2 sorption does not change dramatically with an increase in the amount of nanoclay percentage.

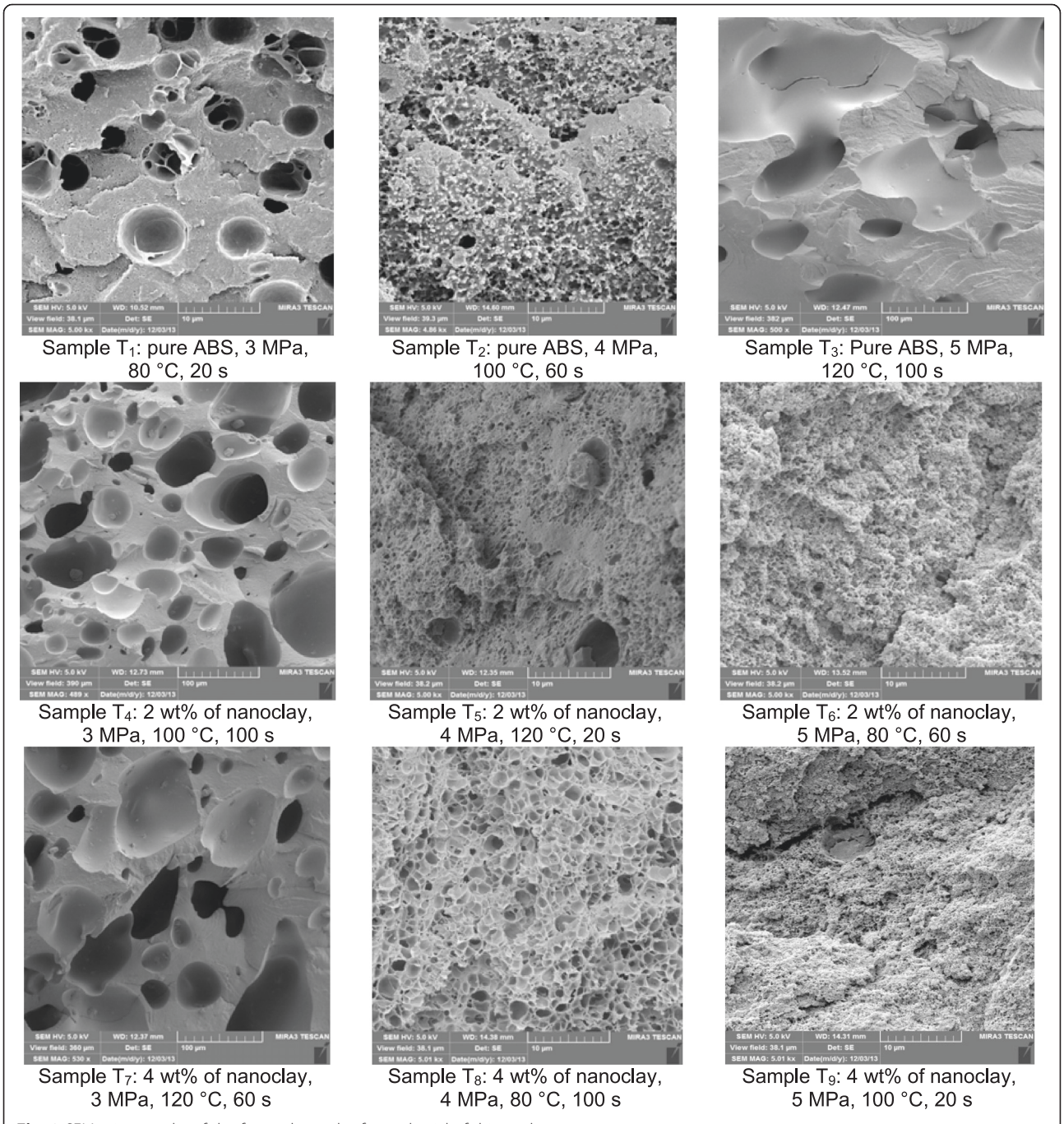

Fig. 9 SEM micrographs of the foamed samples for each trial of this study

Table 10 Results of cell density for foamed samples

Trials	Number of counted cells	Image magnification	Cell density(cells/cm^3)
T_1	90	5000	5.19×10^{10}
T_2	950	4860	1.098×10^{12}
T_3	10	500	1.25×10^{6}
T_4	90	489	4.3×10^{7}
T_5	1900	5000	4.82×10^{12}
T_6	1800	5000	4.2×10^{12}
T_7	37	530	1.2×10^{7}
T_8	1100	5010	2.99×10^{12}
T_9	1600	5010	2.77×10^{12}

and saturation time of 120 h. Then, the pressure was released and the samples have been weighted for 25 h (i.e., 1500 min) and in certain time intervals. Figure 6 shows the desorption behavior of the samples. According to Fig. 6, adding nanoclay to pure ABS cannot act as a barrier to the CO_2 exit and, consequently, will not change the desorption rate of CO_2 significantly.

Structural properties of the foamed samples

Foam density

Densities of the unfoamed pure ABS and APCN samples are presented in Table 5. Obtained foam properties including foam density, relative density, and expansion ratio for each trial of the current experiments are presented in Table 6. Also, signal-to-noise (S/N) ratios for

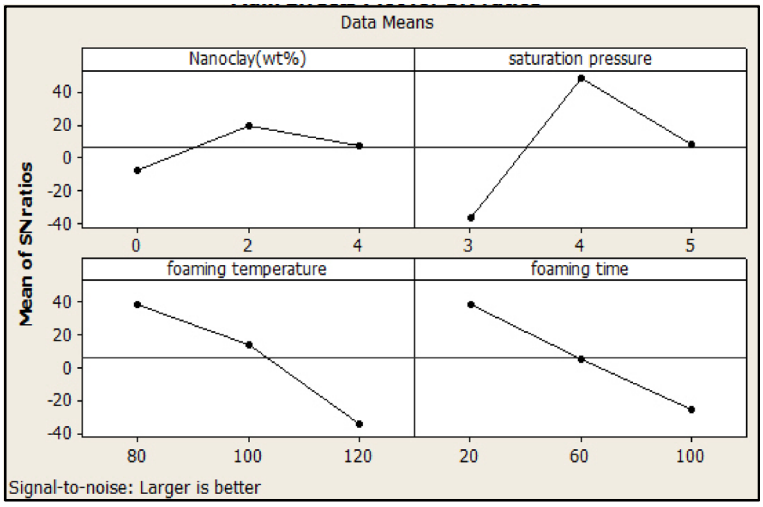

Fig. 10 S/N ratio graphs of process parameters for cell density

Results also reveal that when the saturation pressure increases, the gas uptake is dramatically increased. Although the saturation time was obtained about 100 h from the figures, it is considered 120 h in experimentations to ensure that the samples are fully saturated.

Furthermore, prior to the foaming process, the CO_2 desorption rate of the samples was also obtained in the present study. For this purpose, first, pure ABS and APCN samples were saturated at a saturation pressure of 5 MPa

different levels of parameters are obtained according to Table 7 using Minitab software. In addition, S/N ratio diagrams for process parameters and nanoclay entity are shown in Fig. 7.

Analysis of variance for foam density of samples calculated using Minitab is presented in Table 8, where f is the degrees of freedoms, s is the sum of squares, v is the variance, and P % is the percentage contribution of each parameter (Tang et al. 2007).

Table 11 Cell density results of the confirmation test

Conditions				Results			
Nanoclay (wt%)	Saturation pressure (MPa)	Foaming temperature (°C)	Foaming time (s)	Image magnification	Number of counted cells	Foam density (g/cm^3)	Cell density (cells/cm^3)
0	4	80	20	30,000	37	0.478	3.2×10^{12}
2 (optimal)	4 (optimal)	80 (optimal)	20 (optimal)	30,000	43	0.354	5.6×10^{12}
4	4	80	20	30,000	40	0.42	4.5×10^{12}

Table 12 ANOVA table for foam cell density

Source	*f*	*s*	*v*	*P*%
Nanoclay	2	9.05×10^{24}	4.5×10^{24}	30.2
Saturation pressure	2	15.6×10^{24}	7.84×10^{24}	52.33
Foaming temperature	2	1.57×10^{24}	7.89×10^{24}	5.26
Foaming time	2	3.66×10^{24}	1.83×10^{24}	12.21
Pooled error	0	0	–	–
Total	8	30×10^{24}	–	100

Because of this phenomenon, the sorption/desorption rate is increased. These results are consistent with the reported findings of Laetitia et al. They studied the batch foaming of SAN/clay and showed that the CO_2 sorption/desorption rate reduces for nanocomposites with two kinds of clay nanocomposites, exfoliated clay and intercalated clay. Also, exfoliated clay has a lower sorption/desorption rate due to the perfect dispersion (Urbanczyk et al. 2010). Finally, under the obtained optimal foaming conditions, a confirmation test was performed. The result of the optimal APCN foamed sample is shown in Table 9. As the results show, a larger

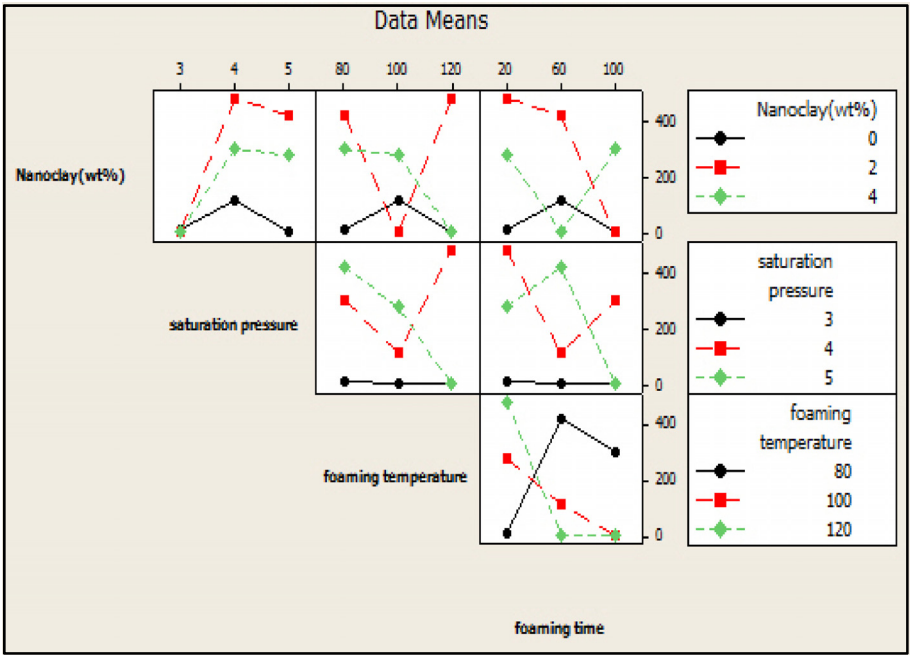

Fig. 11 Interaction plot of factors for sample cell density

One important result that could be obtained from Fig. 7 is the optimum condition of the foaming process with regard to the foam density. As Fig. 7 depicts, foamed samples in the condition of nanoclay percentage of 2 wt %, saturation pressure of 4 MPa, foaming temperature of 80 °C, and foaming time of 100 s have minimum density and, consequently, maximum expansion ratio. Besides this, as shown in Table 8, regarding the foam density, the most effective parameter is foaming temperature with a percentage contribution of 55 %. The optimum foaming temperature of 80 °C is slightly lower than the ABS transition temperature (i.e., 99 °C). When CO_2 dissolves in many polymers, it acts as lubricant; therefore, the chain mobility increases and the polymer glass transition temperature decreases.

Table 13 Average cell size results of APCN foams

Trials	Image magnification	Number of the measured cells	Average cell size (μm)
T_1	5000	15	4.3
T_2	4860	30	0.577
T_3	500	6	55.8
T_4	489	40	27.5
T_5	5000	100	0.41
T_6	5000	100	0.35
T_7	530	30	48
T_8	5010	100	0.87
T_9	5010	100	0.152

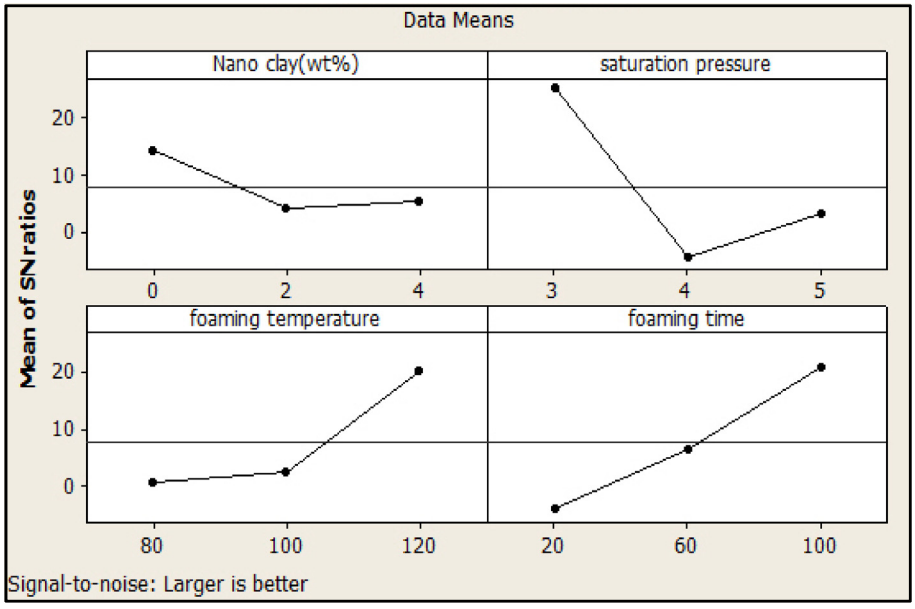

Fig. 12 S/N ratio graphs of process parameters for cell size

decrease in the foam density and consequently larger increase in expansion ratio could be obtained in comparison with all foam results obtained from this study (i.e., results in Table 6).

Figure 8 shows the interaction plot of processing factors for the samples' density. A noticeable result that could be obtained from Fig. 8 is the fact that at medium level of nanoclay percentage (i.e., 2 wt %, which is the optimum level), the foam density does not change significantly with various amounts of processing parameters.

Cell density

In this study, in order to determine cell density of pure ABS and APCN foams, SEM tests were conducted. Captured SEM images are shown in Fig. 9. The calculated cell density from the SEM pictures of each trial is shown in Table 10. Using analysis of Minitab software, the S/N ratio diagram for nanoclay amount and process parameters were obtained and presented in Fig. 10. The optimal foaming conditions and nanoclay amount could be achieved from the S/N ratio graph of Fig. 10. According to Fig. 10, the optimal foaming condition regarding the maximum cell density occurs at a nanoclay percentage of 2 wt %, saturation pressure of 4 MPa, foaming temperature of 80 °C, and foaming time of 20 s.

After finding the optimum condition for cell density, a confirmation test based on this condition was also performed. The calculated cell density from the SEM pictures of this confirmation test is shown in Table 11. In order to observe the effect of the nanoclay on cell density, a comparison of the cell density of the optimal foamed sample (i.e., ABS with 2 wt % nanoclay) with the cell density of the pure ABS and ABS with 4 wt % nanoclay was performed (Table 11). The comparison reveals that an improvement of about 75 % could be achieved in the cell density of foamed samples. Therefore, we can affirm that the nanoclay induces the heterogeneous nucleation agent in the nanocomposite samples' foaming process.

In the next step of our research work, in order to obtain the contribution percentage of the effect of each parameter on the cell density, the analysis of variance for the cell density of APCN foams was calculated and is presented in Table 12. According to Table 12, regarding the cell density, the most effective factors are saturation pressure and nanoclay percentage with percentage contribution (i.e., *P* %) of 52.33 and 30.2 %, respectively. In other words, nanoclay particles can incredibly increase the cell density of foamed samples. The interaction of parameters for the cell density of samples was also studied and then presented in Fig. 11. Regarding the effect of nanoclay content on the cell density of foamed samples, it is concluded from Fig. 11 that at low levels of saturation pressure (i.e., 3 MPa), adding nanoclay did not affect the cell density, while at higher amounts of saturation pressure (i.e., 4 and 5 MPa), adding nanoclay significantly affected the cell density of the foamed

Table 14 Obtained results from confirmation tests for cell size of APCN foams

	Nanoclay percentage (wt%)		
	0	2	4
Average cell size (μm)	63.63	52.83	59.75

Table 15 ANOVA table for APCN foam cell size

Source	*f*	*s*	*v*	*P*%
Nanoclay (wt%)	2	179.75	89.875	4.41
Saturation pressure (MPa)	2	1065.73	532.865	26.13
Foaming temperature (°C)	2	1780.95	890.475	43.66
Foaming time (s)	2	1052.62	526.31	25.8
Pooled error	0	0	–	–
Total	8	4079.04	–	100

samples. Furthermore, in terms of the effect on cell density, an optimum amount for nanoclay was observed (Fig. 11). In other words, adding nanoclay can influence most significantly the cell density when it is in its medium level (i.e., optimum level of 2 wt %).

Cell size

In the foaming process, cell size as an important structural property was measured based on the SEM pictures. The findings from the measurement of cell size for each trial of this research are shown in Table 13. These results were analyzed using Minitab software. Using the analysis from Minitab software, the S/N ratio diagram for nanoclay amount and process parameters could be obtained as shown in Fig. 12. According to Fig. 12, the optimal foaming conditions regarding the maximum cell size are the nanoclay percentage of 0 wt % (pure ABS), saturation pressure of 3 MPa, foaming temperature of 120 °C, and foaming time of 100 s**.** Afterward, nanocomposite samples were foamed under optimal foaming conditions. In order to observe the effect of the nanoclay on cell size, a comparison of the cell size of the optimal foamed sample (i.e., pure ABS) with the cell size of ABS with 2 and 4 wt % nanoclay was performed according to Table 14. The comparison revealed that an increase of about 20 % could be achieved in terms of cell size in foamed samples. According to Table 14, the cell size of foamed samples decreases by adding nanoclay particles. This means that reduction in cell size could be due to the presence of nanoparticles that act as foaming agents which increase the cell numbers and constrain the cell growth. Consequently, the cell size will be decreased.

Analysis of variance (ANOVA) for the cell size of nanocomposite foams was performed according to Table 15. As results show, the most effective factors in terms of the cell size increase are foaming temperature, saturation pressure, and foaming time with a percentage contribution of 43.66, 26.13, and 25.8 %, respectively. As it is clear, when foaming temperature and time increase, since the nanocomposite materials are changed more into dough and cells have more time for expansion, the cell size of the foamed samples will be increased. Regarding the foaming pressure, there is also no doubt that by increasing the gas pressure, the amount of the absorbed gas available for expansion will be increased, and consequently, the cell size increases. Results of Table 15 also state that nanoclay wt % has the least effect on cell size increase. In fact, as it is mentioned previously, nanoclay particles can act as the foaming agents that decrease the cell size of nanocomposite foams. The interaction plot of processing factors for cell size of foamed samples is also shown in Fig. 13. As an interesting

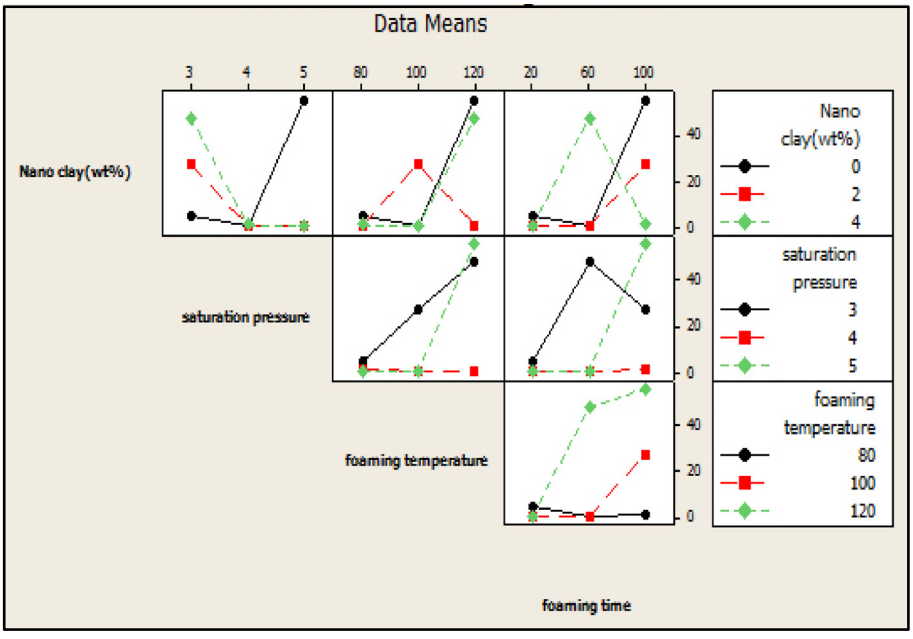

Fig. 13 Interaction plot of processing parameters for sample cell size

result, Fig. 13 reveals that at medium level of saturation pressure (4 MPa), low level of foaming temperature (80 °C), and low level of foaming time (20 s), changing the amount of other parameters does not have a considerable effect on the cell size of nanocomposite samples.

Conclusions

In this research work, ABS/PMMA/clay (APCN) nanocomposites with 2 and 4 wt % of nanoclay were prepared. In order to ensure login polymer chains into nanoclay layers, XRD tests were conducted. The results obtained from XRD tests show that the mixing process has been successfully performed. The CO_2 sorption/desorption rate into the APCN structure in ambient temperature was assessed. Findings show that effective parameters on foam density reduction are foaming temperature, saturation pressure, nanoclay percentage, and foaming time, respectively. According to obtained results, the nanoclay particles increase cell density. Effective parameters on cell density increase are saturation pressure, nanoclay percentage, foaming time, and foaming temperature, respectively. Also, it was found that nanoclay particles are a barrier to cell size expansion in APCN foams. Effective parameters on cell size are foaming temperature, saturation pressure, foaming time, and nanoclay percentage, respectively. Regarding the foam properties, in this study, nanocomposite foam structural properties including foam density, cell density, and cell size were characterized. As it is mentioned in the manuscript, results show that foaming temperature has the most effect on foam density, especially in temperatures lower than and around polymer transition temperature. Also, it is concluded that saturation pressure has the most effect on cell density. After saturation pressure, added nanoclay as a nucleation agent is the most significant parameter on cell density. On the other hand, results show that nanoclay has the least effect on cell size.

Competing interests

The authors declare that they have no competing interests.

Authors' contributions

BA and SMS have foamed the nanocomposite samples of the research work. TA have analyzed the results. AD has performed the Analysis of variance (ANOVA) of the results. REL has revised the paper. However All authors read and approved the final manuscript.

Author details

[1]Mechanical Engineering Department, Faculty of Engineering, Urmia University, Urmia, Iran. [2]Macro Engineering and Technology Inc., Mississauga, Ontario, Canada.

Received: 15 March 2015 Accepted: 19 July 2015
Published online: 06 August 2015

References

Beydokhti, KK, Behravesh, AH, & Azdast, T. (2006). An experimental study on mechanical and microstructural properties of microcellular foams of ABS composites. *Iranian Polymer Journal, 15*(7), 555–567.

Colton, JS, & Suh, NP. (1987). Nucleation of microcellular thermoplastic foam with additives. *Polymer Engineering and Science, 27*, 485–499.

Jacobs, LJM, Kemmere, MF, & Keurentjes, JTF. (2008). Sustainable polymer foaming using high pressure carbon dioxide: a review on fundamental, process and applications. *Green Chem., 10*, 731–738.

James, L, Zeng, C, Cao, X, Han, X, Shen, J, & Xu, G. (2005). Polymer nanocomposite foams. *Composites Science and Technology, 65*, 2344–2363.

Lee, ST, Park, CB, & Ramesh, NS. (2007). *Polymeric foams: science and technology*. Boca Raton, FL: Taylor and Francis.

Mamaghani Shishavan, S, Azdast, T, & Rash Ahmadi, S. (2014). Investigation of the effect of nanoclay and processing parameters on the tensile strength and hardness of injection molded acrylonitrile butadiene styrene-organoclay nanocomposites. *Materials & Design, 58*, 527–534.

Martini, JE (1981) The production and analysis of microcellular foam. Master's thesis in Mechanical Engineering, MIT, http://hdl.handle.net/1721.1/15748.

Murray, RE, Weller, JE, & Kumar, V. (2000). Solid-state microcellular acrylonitrile-butadiene-styrene foams. *Cellular Polymers, 19*, 413–425.

Okamoto, M, Nam, PH, Maiti, P, Kotaka, T, Nakayama, T, Takada, M, Ohshima, M, Usuki, A, Hasegawa, N, & Okamoto, H. (2001). Biaxial flow-induced alignment of silicate layers in polypropylene/clay nanocomposite foam. *Nano Letters, 1*(9), 503–505.

Saraeian, P, Tavakoli, HR, & Ghassemi, A. (2012). Production of polystyrene-nanoclay nanocomposite foam and effect of nanoclay particles on foam cell size. *Journal of Composite Materials, 47*(18), 2211–2217.

Singh, P, & Ghosh, AK. (2014). Torsional, tensile and structural properties of acrylonitrile–butadiene–styrene clay nanocomposites. *Materials and Design, 55*, 137–145.

Tang, SH, Tan, YJ, Sapuan, SM, Suliman, S, Ismail, N, & Samin, R. (2007). The use of Taguchi method in the design of plastic injection mould for reduction warpage. *Journal of Materials Processing Technology, 182*, 418–426.

Urbanczyk, L, Calberg, C, Detrembleur, C, Jerome, C, & Alexandre, M. (2010). Batch foaming of SAN/clay nanocomposites with $scCO_2$: a very tunable way of controlling the cellular morphology. *Polymer, 51*, 3520–3531.

Yeh, JM, Chang, KC, Peng, CW, Lai, MC, Hung, CB, Hsu, SC, Hwang, SS, & Lin, HR. (2009). Effect of dispersion capability of organoclay on cellular structure and physical properties of PMMA/clay nanocomposite foams. *Materials Chemistry and Physics, 115*, 744–750.

Zhai, W, Yu, J, Wu, L, Ma, W, & He, J. (2006). Heterogeneous nucleation uniform zing cell size distribution in microcellular nanocomposite foams. *Polymer, 47*, 7580–7589.